nature geoscience

LETTERS

PUBLISHED ONLINE: 9 MAY 2010 | DOI: 10.1038/NGEO855

Mantle upwellings above slab graveyards linked to the global geoid lows

Sonja Spasojevic[1]*, Michael Gurnis[1] and Rupert Sutherland[2]

The global geoid is characterized by a semi-continuous belt of lows that surround the Pacific Ocean, including isolated minima in the Indian Ocean, Ross Sea and northeast Pacific and west Atlantic oceans. These geoid lows have been attributed to Mesozoic subduction[1,2]. Geodynamic models that include slab graveyards in the lower mantle as inferred from seismic topography or from plate reconstructions correctly predict the general trend of geoid minima[3,4]. However, these models fail to accurately reproduce localized geoid lows in the Indian Ocean, Ross Sea and northeast Pacific Ocean. Here we show that the geoid lows are correlated with high-velocity anomalies near the base of the mantle and low-velocity anomalies in the mid-to-upper mantle. Our mantle flow models reproduce the geoid minima if the mid-to-upper mantle upwellings are positioned above the inferred locations of ancient subducted slabs. We find that the long-wavelength trough in the geoid is linked to high-density slab graveyards in the lower mantle, whereas upwelling regions in the mantle above 1,000 km depth cause discrete lows within the larger trough. We suggest that this mode of upwelling in the mid-to-upper mantle is caused by buoyant hydrated mantle that was created by processes around and above subducted slabs.

The shape of the global geoid is characterized by a semi-continuous 10–30-m-amplitude negative anomaly surrounding the Pacific Ocean, with high-amplitude (-40 to -90 m) localized minima in the Indian Ocean, Ross Sea, northeast Pacific Ocean and west Atlantic Ocean within this trough (Fig. 1a). The more continuous eastern hemisphere low extends from Siberia through India into the Ross Sea. The more segmented western hemisphere low includes a north–south trending anomaly in the northeast Pacific Ocean and a zone that includes Hudson Bay and the western Atlantic Ocean. Localized geoid lows persist after isostatic corrections for the lithosphere have been applied[5]. Analysis of the gravity field as a simultaneous function of position and spectral content[6] shows that about half of the Hudson Bay anomaly could be explained by incomplete postglacial rebound, but such a mechanism cannot explain any significant component of the other geoid lows, because they are not correlated with positions of past ice sheets. The primary explanation for the shape of the geoid is related to heterogeneity and dynamics within the mantle[1–4].

It has previously been noted that geoid lows are globally correlated with locations of Mesozoic subduction[1,2], whereas geoid highs are correlated with present-day subduction zones and hotspots[7]. Active subduction zones are characterized by geoid highs resulting from a dominating positive mass anomaly of cold, upper mantle slabs compared with a low from dynamic topography[8,9]. As slabs sink into the higher-viscosity lower mantle, the dynamic response functions switch sign[9], resulting in an association of lower mantle slabs with negative geoid anomalies. We analysed global tomographic images of seismic velocity to explore the hypothesis that geoid lows are spatially correlated with slab graveyards and high seismic velocities[1,2]. It is clear that geoid lows are indeed underlain by volumes with high seismic velocities near the base of the mantle (Fig. 1b, Supplementary Fig. S1a), but we also find that there are anomalously low seismic velocities in the upper part of the mantle in the same regions (Fig. 1c, Supplementary Fig. S1b). These low-seismic-velocity anomalies are found at depths up to 1,000 km and have absolute amplitudes that are at least as large as the deeper high-velocity anomalies (Fig. 1d).

A global analysis of the correlation between different tomography models and the geoid (Supplementary Fig. S1e) reveals that slow seismic velocities in the upper half of the mantle and fast seismic velocities in the lower half of the mantle are both correlated with geoid lows, whereas geoid highs have a similar strength of correlation with fast seismic velocities in the upper approximately 800 km of mantle (actively subducting slabs) and slow seismic velocities in the lower mantle (inferred to be superplumes and hotspots). The relatively high values of correlation between velocity anomalies and geoid lows, combined with our tectonic interpretations of cross-sections through the tomographic models (Fig. 1e, Supplementary Fig. S1c–d), lead us to suggest that buoyant upwellings above slab graveyards play a significant role in producing the global pattern of geoid lows. Similar suggestions have been made previously to explain regional features of tomography models and the geoid. It was suggested that increased water content in the upper mantle beneath the US east coast[10] was supplied by the subducted Farallon slab and caused an extensive zone of low seismic velocities in the upper mantle. The geoid low between Antarctica and New Zealand is best explained by middle and upper mantle upwelling that followed the cessation of subduction beneath Gondwanaland[11].

To further investigate this hypothesis, we developed instantaneous models of global mantle flow based on density structures scaled from seismic tomography. Previous global geodynamic studies have used the geoid and gravity as constraints on seismic velocity–density scaling, and on mantle viscosity as a function of radius[3,12,13], or more complex functions with radial and lateral parameterizations based on tectonic regionalizations[14,15]. Regional models of the Tonga–Kermadec and Aleutian subduction zones[8,16] show that significant lateral viscosity variations are required between upper mantle slabs and adjacent mantles wedges to match the geoid, whereas some global studies indicate that weak plate margins in the lithosphere are needed to match positive geoid anomalies over subduction zones[14]. Viscosity variation is defined differently for two sets of models: (1) viscosity variation as a function of radius and temperature; and (2) lateral viscosity variation in the upper mantle based on tectonic regionalization in addition to radial and temperature viscosity

[1]Seismological Laboratory, California Institute of Technology, Pasadena, California 91125, USA, [2]GNS Science, PO Box 30368, Lower Hutt 5040, New Zealand. *e-mail: sonja@gps.caltech.edu.

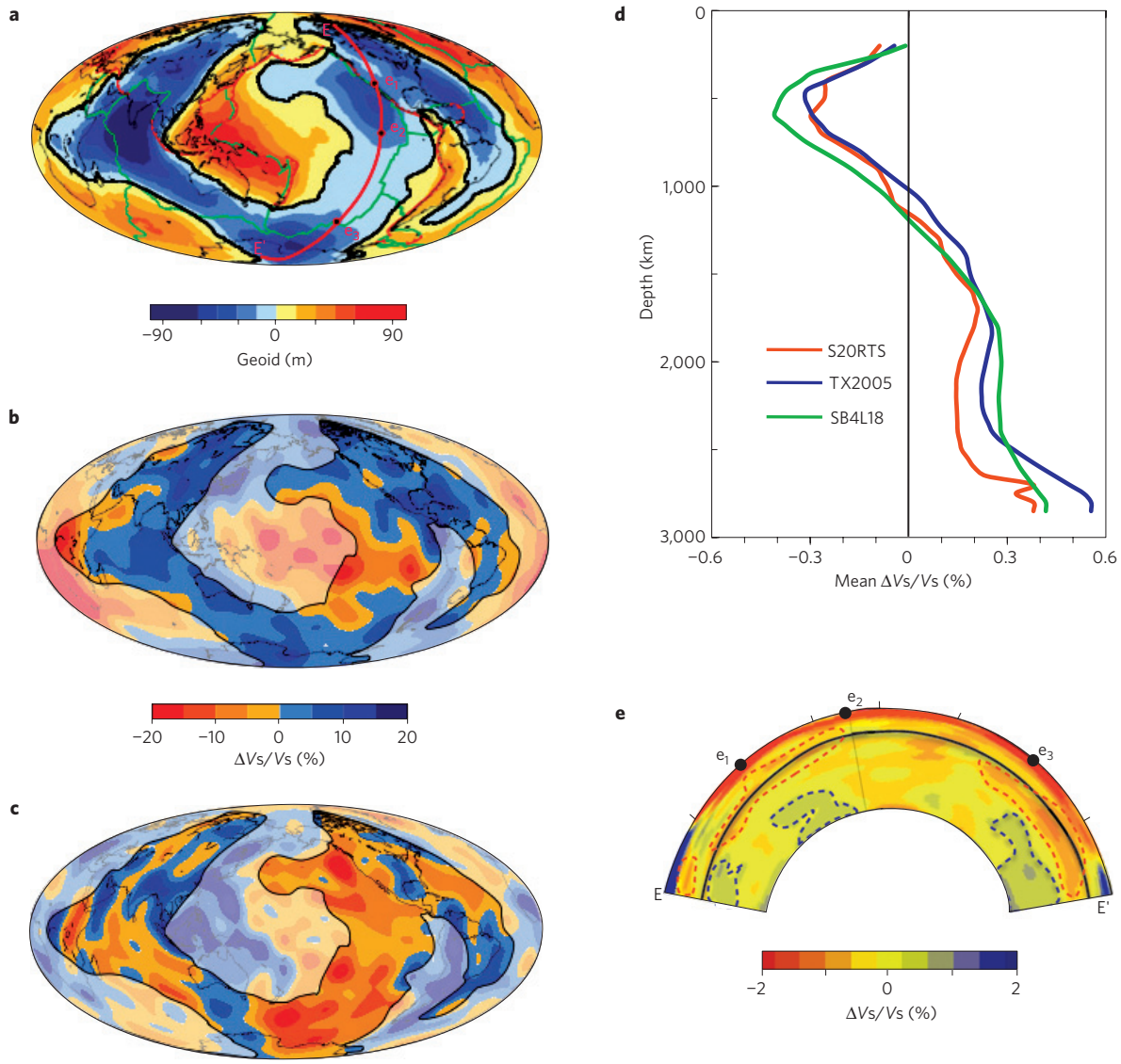

Figure 1 | Relationship between the geoid and seismic tomography. a, Observed geoid. **b**,**c**, Integrated S20RTS (ref. 17) tomographic images for depth ranges 2,000–2,890 km (**b**) and 300–1,000 km (**c**). **d**, Difference in the mean value of the wave-speed anomaly[17–19] between localized geoid lows (<−30 m) and global tomography for different tomographic models. **e**, Cross-section through the S20RTS (ref. 17) model. Tomography (**b**,**c**) is integrated at every 50 km; the semi-transparent overlay covers the area of positive geoid anomaly; and the cross-section position is shown in **a** by a red line; the dashed blue and red lines in **e** represent high-velocity lower mantle and low-velocity mid-upper mantle anomalies respectively.

variation (Supplementary Fig. S2). Acceptable geoid predictions are made by both classes of models (Supplementary Fig. S3), and all of the best-fitting models have a viscosity increase across the 660 km discontinuity of a factor of 80–100. Different seismic-tomographic inputs result in geoid predictions of varying success in different parts of the world (Supplementary Fig. S4). Model S20RTS (ref. 17) as input yields better predictions in the Pacific Ocean and circum-Pacific region, SB4L18 (ref. 18) fits the region extending from the North Atlantic Ocean to south of Africa and TX2005 (ref. 19) best predicts the Indian Ocean geoid low (Supplementary Fig. S4). The choices of different tomographic models as input, and alternative models of lateral and vertical viscosity variation, have relatively greater impacts on geoid predictions than the choice of seismic velocity-to-density scaling relationship (Supplementary Fig. S5).

The best-fitting model (Fig. 2a) was found by a systematic parameter search (Supplementary Figs 1–5). The eastern hemisphere geoid low is predicted as a relatively continuous structure with distinct Ross Sea minima. Two separate geoid lows emerge in the western hemisphere in the northeast Pacific and western Atlantic oceans. The amplitudes of the Ross Sea and northeast Pacific Ocean geoid minima are predicted well, whereas the Indian Ocean low is systematically under predicted, which could be attributed to poor regional sampling by seismic body waves.

To investigate the importance of mantle upwellings, we removed the low-density anomalies in the upper- to mid-mantle depth range (Fig. 2b,c). With positive buoyancy variations shallower than 1,000 km depth removed, predictions of localized geoid minima in the northeast Pacific Ocean and Ross Sea regions disappear (Fig. 2c). The largest negative geoid anomaly in the Indian Ocean remains, but the amplitude is reduced. We could not find a model with reasonable seismic velocity–density scaling (Supplementary Fig. S5) that reproduces the observed amplitudes of geoid minima with only lower mantle slabs. Therefore, we conclude that buoyant upwellings above about 1,000 km depth cause localized high-amplitude geoid minima, and the longer-wavelength geoid trough of amplitude −10 to −30 m that surrounds the Pacific Ocean

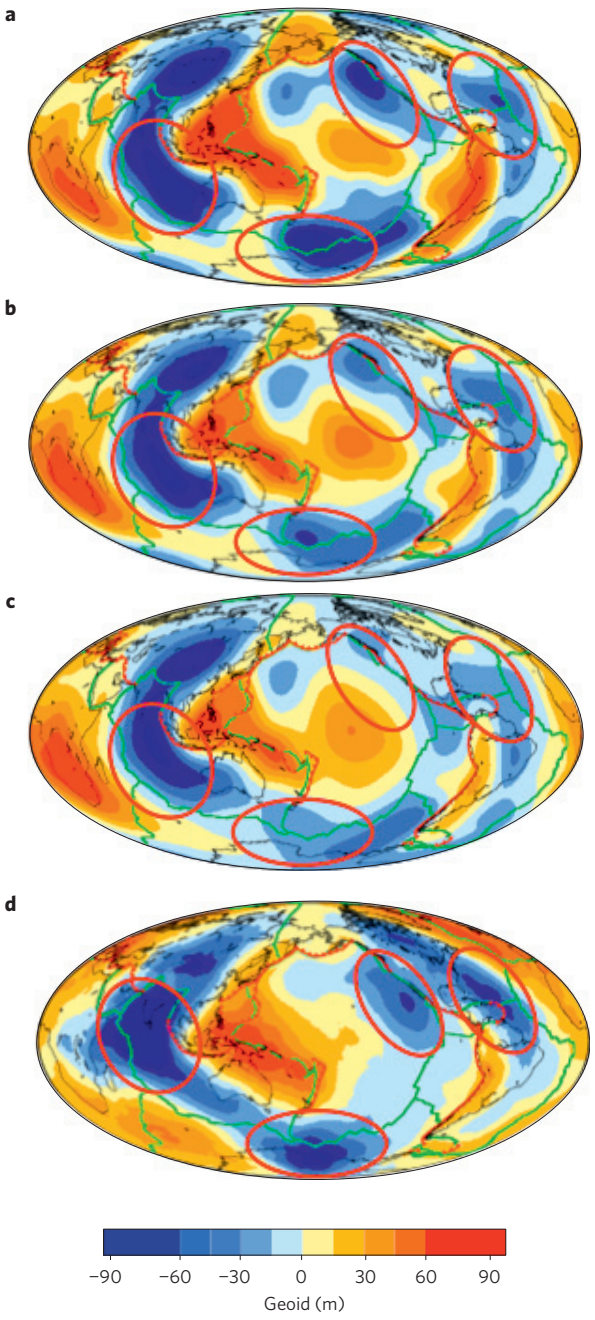

Figure 2 | Predicted and observed geoid. a, Geoid prediction for the best-fitting model ($C_1 = 0.61$; $C_2 = 0.79$). **b**,**c**, Geoid prediction for the best model with upwellings removed in depths 0–660 km ($C_1 = 0.60$; $C_2 = 0.74$) (**b**) and 0–1,000 km ($C_1 = 0.59$; $C_2 = 0.71$) (**c**). **d**, Observed geoid. See Supplementary Fig. S3b,g for the radial viscosity structure and seismic velocity–density scaling (viscosity ratio at 660 km is 1:100). All buoyancy anomalies are scaled from S20RTS tomography[17]. Correlation coefficients C_1 and C_2 between the predicted and observed geoid are calculated for the whole Earth's surface (C_1) and the region of geoid low (C_2). The red ellipses indicate four zones of localized geoid minima.

is related to accumulations of high-density Mesozoic slabs near the base of the mantle.

The negative geoid anomaly in the northeast Pacific appears to be due to upwelling located in the upper-to-mid mantle (Fig. 2; Supplementary Table 1), and we suggest a possible causal relationship between this upwelling and lowermost mantle high-velocity material (Fig. 1e, Supplementary Fig. S1c). If this high-velocity material is related to ancient subduction, it is substantially west of the Farallon slab[20], and the exact timing and origin of its subduction zone source is unknown. For the Ross Sea geoid low, about 40% of the predicted low disappears as upwellings are stripped out of the upper mantle (Fig. 2b; Supplementary Table 1), and only 40% of the geoid low remains once the upwellings are removed in the upper 1,000 km (Fig. 2c, Supplementary Table 1). We have previously proposed that anomalously high topography of Ross Sea to Marie Byrd Land region, excess Campbell plateau subsidence and the geoid low in the Ross Sea are causally related to low-density material above the Gondwana slab graveyard in this region[11,21].

The Indian Ocean geoid low is not fitted well by models that reproduce other geoid anomalies, but models do show that about 20% of the predicted anomaly is related to mantle structure shallower than 1,000 km (Supplementary Table 1). The position of the Indian Ocean geoid low corresponds to the reconstructed position of Tethyan subduction[22]. It is possible that an upwelling was created by interaction of this slab with the upper-to-mid mantle, as implied by the TX2005 (ref. 19) model (Supplementary Fig. S1). Such an upwelling may not be well imaged by tomographic models, but could explain the relatively small Cenozoic subsidence of India[23], as compared with that expected from movement over a mantle downwelling, such as the observed subsidence of Australia[24] and North America[25]. If the upwelling was located above the subducting slab when India drifted northward, the dynamic effects of these two opposing anomalies could cancel and India would not experience significant subsidence or uplift, consistent with the record of limited marine flooding on the Indian continent[23].

The western Atlantic Ocean geoid signal is complicated by incomplete postglacial rebound in North America, with our geodynamic models predicting a geoid low to be more spatially constrained than the observed geoid low (Fig. 2). However, tomography inversions reveal an extensive zone of low seismic velocities in the upper mantle along the US east coast[10] located above the subducted Farallon slab. The upwelling in the western Atlantic Ocean along the US east coast has previously been attributed to increased water content in the upper mantle, probably supplied by subduction of the Farallon slab[10]. Our models indicated that about 40% of the geoid low in the western Atlantic Ocean results from upper-to-mid mantle low-density upwellings (Fig. 2; Supplementary Table 1).

As the low-density material that we identify is often above ancient subducted slabs, we suggest that it is causally related. We propose that the low density of the mantle in these regions could be a result of phase separation (for example, melting), hydration reactions or some other form of chemical alteration by ancient subducted slabs. This hypothesis is supported by mineral physics studies that have investigated phase relationships in the olivine–water system[27] and the mantle[28] water storage capacity. Experimental studies on the effects of water on the kinetics of the olivine–wadsleyite system[27] indicate that, in addition to the mantle wedge in subduction zones and the mantle transition zone, two dehydration sites exist in the lower mantle: the top of the lower mantle where hydrous ringwoodite and superhydrous phase B decompose, and 1,200–1,500 km depth where phase D(G) decomposes. However, at present, as far as we are aware, there are no mineral physics studies that link the amount of water in the upper reaches of the lower mantle to perturbations in seismic velocities.

Our models confirm that deep slab graveyards are responsible for the long-wavelength geoid trough. We also find evidence for low-density mantle upwellings at upper-to-mid mantle depths above this region of subducted Mesozoic slabs, and confirm them to be a primary cause of high-amplitude intermediate-wavelength geoid minima within the global belt of geoid lows. We could

not construct a model with reasonable velocity-to-density scaling and viscosity structure that reproduced localized geoid minima without these low-density upwellings in the upper 1,000 km of the mantle. Although recognized in regional studies of the US east coast[10] and the Antarctica–New Zealand conjugate margins[11,21], such upwellings have not previously been investigated globally and we propose that they constitute a previously unrecognized mode of mantle upwellings[26] that is causally related to the activity of ancient subduction zones.

Methods

We develop instantaneous models of mantle convection using the finite element code CitcomS version 3.1 (ref. 29), which solves the equations of mass, momentum and energy for an incompressible, Newtonian fluid, while making the Boussinesq approximation. We calculate the dynamic topography and geoid accounting for the effect of self-gravitation using a no-slip surface boundary condition. The background mantle is defined as isothermal with a non-dimensional temperature of 0.5, and thermal anomalies are defined with respect to the background mantle by combining seismic tomography in the whole mantle and a synthetic slab model in the upper mantle. Lower mantle thermal anomalies are always defined by appropriate scaling of seismic tomography (Supplementary Fig. S5). Upper mantle cold downwelling anomalies are defined either by appropriate scaling of positive seismic tomography anomalies or from contours of Benioff zone seismicity used in the regionalized upper mantle seismic model[30], whereas upper mantle hot upwelling anomalies are scaled negative seismic anomalies. Seismic velocity-to-density scaling follows a similar approach to previous studies[3,12], and we assume that all buoyancy anomalies are thermal in origin and calculate the temperature anomaly using constants defined in Supplementary Table 1, a depth-independent value of the coefficient of thermal expansion and a depth-dependent scaling. Mantle background viscosity is defined as four layers, which is modified by tectonic regionalization and temperature dependence (Supplementary Fig. S2). The resolution of the models is approximately 50 km, as we use 129×129 nodes per CitcomS cap in map view, and 65 nodes in the vertical direction. Resolution tests are shown in Supplementary Fig. S6. Parameters that remained constant in the model runs are shown in Supplementary Table S2.

Received 27 October 2009; accepted 31 March 2010; published online 9 May 2010

References

1. Chase, C. G. & Sprowl, D. R. The modern geoid and ancient plate boundaries. *Earth Planet. Sci. Lett.* **62,** 314–320 (1983).
2. Richards, M. & Engebretson, D. Large-scale mantle convection and the history of subduction. *Nature* **355,** 437–440 (1992).
3. Steinberger, B. Slabs in the lower mantle—results of dynamic modelling compared with tomographic images and the geoid. *Phys. Earth Planet. Inter.* **118,** 241–257 (2000).
4. Hager, B. H. & Richards, M. A. Long-wavelength variations in Earth's geoid—physical models and dynamic implications. *Phil. Trans. R. Soc. A* **328,** 309–327 (1989).
5. Kaban, M. K., Schwintzer, P. & Reigber, C. A new isostatic model of the lithosphere and gravity field. *J. Geodesy.* **78,** 368–385 (2004).
6. Simons, M. & Hager, B. Localization of the gravity field and the signature of glacial rebound. *Nature* **390,** 500–504 (1997).
7. Richards, M. A., Hager, B. H. & Sleep, N. H. Dynamically supported geoid highs over hotspots—observation and theory. *J. Geophys. Res.* **93,** 7690–7708 (1988).
8. Billen, M. I., Gurnis, M. & Simons, M. Multiscale dynamics of the Tonga–Kermadec subduction zone. *Geophys. J. Int.* **153,** 359–388 (2003).
9. Richards, M. A. & Hager, B. H. Geoid anomalies in a dynamic Earth. *J. Geophys. Res.* **89,** 5987–6002 (1984).
10. van der Lee, S., Regenauer-Lieb, K. & Yuen, D. A. The role of water in connecting past and future episodes of subduction. *Earth Planet. Sci. Lett.* **273,** 15–27 (2008).
11. Sutherland, R., Spasojevic, S. & Gurnis, M. Mantle upwelling after Gondwana subduction death may explain anomalous topography of West Antarctica and subsidence history of eastern New Zealand. *Geology* **38,** 155–158 (2009).
12. Forte, A. M. & Mitrovica, J. X. Deep-mantle high-viscosity flow and thermochemical structure inferred from seismic and geodynamic data. *Nature* **410,** 1049–1056 (2001).
13. Steinberger, B. & Calderwood, A. R. Models of large-scale viscous flow in the Earth's mantle with constraints from mineral physics and surface observations. *Geophys. J. Int.* **167,** 1461–1481 (2006).
14. Yoshida, M. & Nakakuki, T. Effects on the long-wavelength geoid anomaly of lateral viscosity variations caused by stiff subducting slabs, weak plate margins and lower mantle rheology. *Phys. Earth Planet. Inter.* **172,** 278–288 (2009).
15. Cadek, O. & Fleitout, L. Effect of lateral viscosity variations in the top 300 km on the geoid and dynamic topography. *Geophys. J. Int.* **152,** 566–580 (2003).
16. Billen, M. I. & Gurnis, M. A low viscosity wedge in subduction zones. *Earth Planet. Sci. Lett.* **193,** 227–236 (2001).
17. Ritsema, J., van Heijst, H. J. & Woodhouse, J. H. Global transition zone tomography. *J. Geophys. Res.* **109,** B02302 (2004).
18. Masters, G., Laske, G., Bolton, H. & Dziewonski, A. in *The Relative Behaviour of Shear Velocity, Bulk Sound Speed, and Compressional Velocity in the Mantle: Implications for Chemical and Thermal Structure* (eds Karato, S. I. *et al.*) 63–88 (Geophysical Monograph Series, Vol. 117, American Geophysical Union, 2000).
19. Simmons, N. A., Forte, A. M. & Grand, S. P. Constraining mantle flow with seismic and geodynamic data: A joint approach. *Earth Planet. Sci. Lett.* **246,** 109–124 (2006).
20. Grand, S. P. Mantle shear-wave tomography and the fate of subducted slabs. *Phil. Trans. R. Soc. A* **360,** 2475–2491 (2002).
21. Spasojevic, S., Gurnis, M. & Sutherland, R. Inferring mantle properties with an evolving dynamic model of the Antarctica–New Zealand region from the Late Cretaceous. *J. Geophys. Res.* (in the press, 2010).
22. Aitchison, J. C., Ali, J. R. & Davis, A. M. When and where did India and Asia collide? *J. Geophys. Res.* **112,** B05423 (2007).
23. Fleitout, L. & Singh, R. N. *17th Math. Geophys. Con.* 143 (1988).
24. Gurnis, M., Müller, R. & Moresi, L. Cretaceous vertical motion of Australia and the Australian–Antarctic discordance. *Science* **279,** 1499–1504 (1998).
25. Spasojevic, S., Liu, L. J. & Gurnis, M. Adjoint models of mantle convection with seismic, plate motion, and stratigraphic constraints: North America since the Late Cretaceous. *Geochem. Geophys. Geosyst.* **10,** Q05W02 (2009).
26. Courtillot, V., Davaille, A., Besse, J. & Stock, J. Three distinct types of hotspots in the Earth's mantle. *Earth Planet. Sci. Lett.* **205,** 295–308 (2003).
27. Ohtani, E., Litasov, K., Hosoya, T., Kubo, T. & Kondo, T. Water transport into the deep mantle and formation of a hydrous transition zone. *Earth Planet. Sci. Lett.* **143–144,** 255–269 (2004).
28. Hirschmann, M. M. Water, melting, and the deep Earth H_2O cycle. *Annu. Rev. Earth Planet. Sci.* **34,** 629–653 (2006).
29. Tan, E., Choi, E., Thoutireddy, P., Gurnis, M. & Aivazis, M. GeoFramework: Coupling multiple models of mantle convection within a computational framework. *Geochem. Geophys. Geosyst.* **7,** Q06001 (2006).
30. Gudmundsson, O. & Sambridge, M. A regionalized upper mantle (RUM) seismic model. *J. Geophys. Res.* **103,** 7121–7136 (1998).

Acknowledgements

We thank R. Moucha for helpful comments on an earlier version of the letter. This work was supported through Caltech Tectonics Observatory (by the Gordon and Betty Moore Foundation), the National Science Foundation (EAR-0609707 and EAR-0810303), the New Zealand Foundation for Research Science and Technology, and StatoilHydro. The original CitcomS software was obtained from CIG, Computational Infrastructure for Geodynamics (http://geodynamics.org). This is Contribution Number 10034 of the Division of Geological and Planetary Sciences and Number 217 of the Tectonics Observatory, Caltech.

Author contributions

S.S. carried out analysis and mantle convection modelling, and all authors participated in the modelling strategy, interpretation of results and preparing the manuscript.

Additional information

The authors declare no competing financial interests. Supplementary information accompanies this paper on www.nature.com/naturegeoscience. Reprints and permissions information is available online at http://npg.nature.com/reprintsandpermissions. Correspondence and requests for materials should be addressed to S.S.